Textile & Leather Review

ISSN 2623-6281| www.tlr-journal.com | 10.31881/TLR

Blow-Room Cotton Waste-Derived Activated Carbon for Supercapacitor Electrodes

Reem Shahin, Alexey Rodin

How to cite: Shahin R, Rodin A. Blow-Room Cotton Waste-Derived Activated Carbon for Supercapacitor Electrodes. Textile & Leather Review. 2026; 9:1016-1035. https://doi.org/10.31881/TLR.2026.1016

How to link: https://doi.org/10.31881/TLR.2026.1016

Published: 27 April 2026

Blow-Room Cotton Waste-Derived Activated Carbon for Supercapacitor Electrodes

Reem Shahin[1*], Alexey Rodin[1,2]

[1]Department of Physical Chemistry, National University of Science and Technology MISIS, 119049 Moscow, Russia

[2] Department of Nanomaterials and Nanotechnology, Mendeleev University of Chemical Technology, 125047 Moscow, Russia

*m2011265@edu.misis.ru

Article

https://doi.org/10.31881/TLR.2026.1016

Received 9 December 2025; Accepted 24 February 2026; Published 27 April 2026

ABSTRACT

Cotton-based waste has increased with the expansion of the textile industry, and despite its rich cellulose content, a large amount of it is thrown away. Simultaneously, the increasing need for high-performance and sustainable energy storage devices has drawn attention to activated carbon (AC) generated from biomass as supercapacitor electrode materials. Converting cotton waste into AC provides an environmentally friendly path to produce useful electrode materials. In this study, blow-room cotton waste was chemically activated using phosphoric acid (H_3PO_4) at two concentrations (50 and 85 wt%) to examine its influence on yield, morphology, and electrochemical behavior. After impregnation and carbonization at 600 °C, the resulting powders were labeled AC-50 and AC-85. Increasing H_3PO_4 concentration reduced activation yield from 24.7 wt% to 20.8 wt% and volatile matter from 9.3 to 6.1 wt%, while increasing fixed carbon and ash content. FT-IR indicated the loss of cellulose features and stronger P–O/P=O bands for AC-85, suggesting deeper phosphorylation. SEM revealed the extensively interconnected pore network for AC-85. Electrodes prepared using AC samples were tested in symmetrical CR2025 cells with 1 M KNO3. Cyclic voltammetry and galvanostatic charge–discharge confirmed electric double-layer behavior, with AC-85 achieving higher capacitance (135.6 F g^{-1} at 1 mV s^{-1}) and better rate performance. Ragone data and EIS further showed lower resistance and improved ion transport for AC-85. Overall, concentrated H_3PO_4 produces AC with richer surface functionality, and superior electrochemical performance, highlighting a potential route to convert blow-room cotton waste into promising electrode materials for supercapacitors.

KEYWORDS

cotton waste, activated carbon, chemical activation, phosphoric acid, supercapacitor electrodes

INTRODUCTION

Global textile production has expanded rapidly in recent decades, driven by population growth and changing consumer preferences, which has contributed to an increase in global fiber consumption and the generation of significant amounts of textile waste [1,2]. Worldwide fiber production reached about 113 million tonnes in 2021 and is expected to rise to 149 million tonnes by 2030, with cotton representing nearly one-quarter, making it the second most significant fiber that year[2]. This boom in production generates enormous waste: an estimated 106 million tonnes of textile solid waste are produced each year. In particular, the surge in cotton output has yielded massive cotton fiber residues [3]. Most of this manufacturing waste is not recycled – on the order of 75% of textile waste ultimately ends up in landfills or is incinerated, causing environmental harm [1].

Within the textile industry, waste is classified as either production (pre-consumer) or post-consumer. Spinning mills generate substantial pre-consumer cotton waste during processing. For example, when raw cotton bales are opened and cleaned in the blow-room stage, a fluffy by-product of short fibers, dust and seed particles is produced [4]. This waste consists of the impurities and short fibers removed in the initial bale-cleaning step. It is regarded as a “garbage” waste that must be cleaned. In practice, blow-room waste is highly contaminated and of low fiber quality, so it is seldom recycled into regular yarns [4,5]. Instead, it is typically used for only very low-value purposes (for example, as stuffing or filler), or disposed contributing to landfill and emissions [4].

Some uses of cotton-processing residues have been explored. Lower-grade cotton trimmings and slivers can sometimes be blended into coarse yarns or nonwoven products [5]. Recent work by Habib et al. (2024) even demonstrated that pre-consumer hard waste can be used to produce rotor yarns suitable for denim [2]. However, the very short, dusty fibres characteristic of blow-room waste generally fall below the threshold for conventional textile recycling, leaving them without a viable high-value reuse pathway [5,6]. These fibers are a lignocellulosic biomass composed of approximately 59.04 % cellulose, 15.27 % hemicellulose, and 7.56 % lignin on a dry-weight basis [7]. The high cellulose content renders them a promising precursor for carbon materials. Porous carbons made from textile wastes have already shown promise in adsorption and electrochemical applications [8]. Production of activated carbon and activated carbon fibres from cotton and general textile wastes has been demonstrated in the literature, with reports of high surface areas and

favourable pore size distributions suitable for adsorption and energy storage [8,9]. In recent years, many forms of biomass have been converted into AC for applications such as adsorption or energy storage, including coconut shell [10], rice husk [11], and agricultural residues [12]. Notably, cotton-based precursors have been used to prepare AC. For instance, Zhao et al. (2020) treated waste cotton fabric with concentrated phosphoric acid (H_3PO_4) and obtained a highly porous AC with strong adsorption properties. Such results suggest that cotton waste – even low-grade waste – can yield valuable porous carbon materials when activated by H_3PO_4 [13].

Activated carbon is commonly produced by chemical activation (impregnating the raw material with a reagent like H_3PO_4, ZnCl or KOH followed by heating) or physical activation (pyrolysis followed by oxidizing treatment) [9-13]. The electrochemical performance of activated carbon strongly depends on the activation process and testing conditions; for example, commercial YP-80F prepared from coconut shells has demonstrated an energy density of around 13.1 $Wh \cdot kg^{-1}$ in KNO_3-based electrolyte systems [14], while nanoporous carbon derived from polypyrrole has achieved approximately 12.4 $Wh \cdot kg^{-1}$ in 2.5 M KNO_3 [15], highlighting the potential of optimized activated carbon structures for efficient energy storage. Phosphoric acid is one of the most widely used chemical activating agents for biomass. During H_3PO_4 activation, the acid catalyzes dehydration, condensation, carbonization, and aromatization of cellulose and other biomass components, forming cross-linked structures that prevent shrinkage of cell walls and facilitate the development of hierarchical pores, predominantly micropores, with some mesoporosity in the resulting carbon [16,17]. Compared to physical activation (steam or CO_2) or other chemical agents such as KOH and $ZnCl_2$, H_3PO_4 activation occurs at lower temperatures (400–600 °C), reducing energy consumption and facilitating easier handling. Moreover, it is non-toxic and readily recoverable, producing fewer hazardous byproducts than alkaline or metal salt activators, and thus offers a more environmentally friendly route for preparing high-surface-area carbon with excellent pore structure [13,18]. The acidic nature and mild oxidizability of H_3PO_4 play key roles in reconstructing the biomass structure and generating additional pores, which in turn enhance the surface area of the activated carbon [16]. The resulting biomass-derived AC typically has a high surface area and good conductivity. Such carbon materials are especially useful as electrodes in supercapacitors, which require high surface-area carbons to achieve large electrical double-layer capacitance [16,17]. Indeed, carbon-based electrodes derived from biomass are considered promising

for supercapacitors because of their low cost, renewability, and eco-friendly nature. Prior studies have demonstrated that activated carbon from rich cellulose waste can deliver high specific capacitance in energy storage cells [19]. These findings motivate the use of textile residues to make supercapacitor materials.

In this work, the preparation of AC from blow-room waste using the direct chemical activation with H_3PO_4 was studied. The effect of two different acid concentrations on the material properties and electrochemical performance was investigated when the prepared AC samples were used as supercapacitor electrodes.. This approach demonstrates a promising pathway for recycling cotton industry waste into energy storage devices.

EXPERIMENTAL

Materials and Methods

Materials

Cotton wastes were obtained from the Yartsevsky Cotton Mill (Russia) and used as a biomass precursor. Phosphoric acid (H_3PO_4, 85%, GOST 6552-80, Russia) was used as the activating agent. Polytetrafluoroethylene suspension (PTFE, 35% solids, Russia) was used as the binder, and CABOT® Vulcan XC72 carbon black (USA) was used as the conductive additive. A 1 M solution of potassium nitrate (KNO_3, GOST 4217-77, Russia) was used to prepare the electrolyte. All reagents were of analytical grade and were used without further purification. CR2025 cells (China) and TF-40-30 dielectrics (Japan) were used to assemble the supercapacitors.

Preparation of Activated Carbon

Chemical activation of cotton waste was carried out using H_3PO_4 solutions of different concentrations (50% and 85% wt) to study the effect of acid concentration on the properties of the AC samples. For this purpose, 30 g of cotton waste was washed and dried, then soaked in 100 ml of H_3PO_4 solution for 24 h, to allow complete acid penetration into the lignocellulosic fibers, after which the samples were dried at 100 °C for 24 h [16,17].

The dried materials were carbonized in a tubular furnace at 600 °C under nitrogen atmosphere (flow rate of 70 mL min^{-1}), where the catalytic action of H_3PO_4 facilitated the decomposition of the organic matrix and the formation of a developed porous structure. The resulting AC was repeatedly washed with hot distilled water

until pH ≈ 7 was reached, which indicated complete removal of acid residues and ensured neutralization of the AC to prevent the influence of residual acid on electrochemical tests. Neutralized samples were dried and ground to a powder state, which increased the specific surface area and facilitated the preparation of electrodes. All stages of the preparation process are summarized in Figure 1.

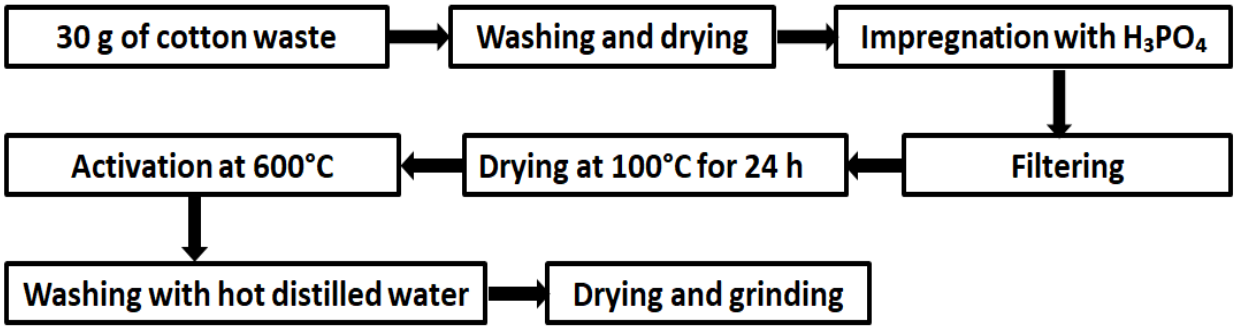

Figure 1. Flowchart of activated carbon preparation

The obtained AC samples were labeled as AC-50 and AC-85, corresponding to samples prepared using 50 wt% and 85 wt% H_3PO_4, respectively. The yield of activation was calculated using Eq. 1:

$$\text{Yield} = \frac{w_{AC}}{w_{CW}} * 100\% \quad (1)$$

Where w_{AC} is the weight of dried activated carbon after washing and w_{CW} is the weight of cotton waste [20].

Electrode Fabrication and Assembly of Symmetrical Supercapacitors

The electrodes were prepared using the prepared samples. AC, carbon black and PTFE were mixed in a mass ratio of 80:10:10. The resulting mixture was dispersed in a solvent to form a homogeneous suspension, which was filtered and then rolled on a roller mill to obtain thin and uniform layers. Electrodes were cut to 12 mm diameter, with an active mass loading of around 5 mg cm^{-2}, and used to assemble symmetrical supercapacitors in which two identical electrodes were separated by a TF-40-30 separator in a CR2025 cell, and 1 M KNO_3 solution was used as the electrolyte.

Characterization

ASTM standards were used to calculate the moisture content (oven-drying method) [21], volatile matter [22], ash content [23] and the fixed carbon of the prepared AC samples. The surface functional groups of the obtained activated carbons were analysed by Fourier transform infrared (FT-IR) spectroscopy using a Nicolet iS20, Thermo Scientific spectrometer with SMART OMNI Transmission accessory in the 4000-400 cm^{1} range. Discs were prepared by mixing the dried powder with KBr in an agate mortar, and the mixture was then compressed at 5 tons cm^{-2} for 5 min. The pore morphology and structure were studied using a Tescan VEGA3 scanning electron microscope at different magnifications. The electrochemical properties of the activated carbons were studied by cyclic voltammetry (CV), galvanostatic charge–discharge (GCD) spectroscopy, and electrochemical impedance spectroscopy (EIS) using a galvanostatic potentiostat P-20X8 multichannel potentiostat (Elins, Russia).

RESULTS AND DISCUSSION

Yield and Proximate Analysis

To study the effect of phosphoric acid concentration on carbonization behavior and material quality, the proximate composition and yield of activated carbon samples were determined. The obtained results are presented in Table 1.

Table 1. Proximate analysis of AC samples

Yield and proximate analysis (wt%)	AC-50	AC-85
Yield	24.7	20.8
Moisture content	2.8	1.9
Ash content	3.1	4.4
Volatile matter	9.3	6.1
Fixed Carbon	84.8	87.6

According to the results found in the table, the yield of AC dropped from 24.7% to 20.8% as the phosphoric acid concentration increased. This observation is a well-established characteristic of chemical activation using phosphoric acid since concentrated H_3PO_4 helps with increasing the hydrolytic cleavage of cellulose and hemicellulose, resulting in enhanced solubility of organic components during the impregnation phase[16,17]. The low moisture content of both samples suggested minimal water adsorption and efficient drying. With increasing acid concentration, the volatile matter content decreased markedly from 9.3% to 6.1% for AC-85. The lower volatile fraction of AC-85 reflects a greater removal of organic matter, resulting in a more thermally and electrically stable activated carbon. At the same time, increasing the acid concentration leads to an increase in the fixed carbon, indicating a higher degree of carbonization in the AC-85 sample. AC-85 exhibits a slightly higher ash content, which may be attributed to residual phosphorus-containing species that were not removed during washing. These results are well aligned with earlier reports, confirming that increasing the H_3PO_4 concentration typically decreases yield while enhancing fixed carbon content and ash formation [24].

FTIR Analysis

The FTIR spectra of raw cotton waste and the two prepared activated carbon samples (AC-50 and AC-85) are presented in Figure 2.

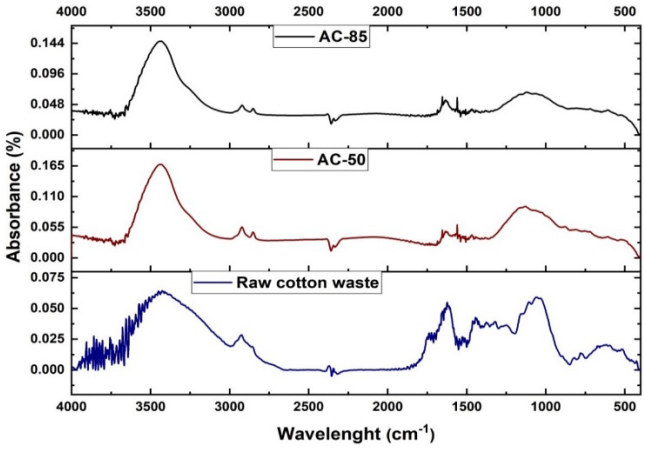

Figure 2. FTIR spectra of cotton waste and the prepared AC samples

The FTIR spectrum of the raw cotton waste displays the well-known spectral fingerprint of cellulose: a broad O–H stretching envelope centered near 3400 cm^{-1} which arises from O-H stretching vibrations of water,

alcohol, carboxyl, and phenol groups [25-27], a peak around 2920 cm^{-1} corresponds to the stretching vibration of aliphatic C-H [26], two peaks around 1735 cm^{-1} and 1633 cm^{-1} assigned to C=O stretching [27] and C=C stretching [25-27], respectively. A cluster of diagnostic cellulose bands in the fingerprint region (1430, 1340, 1160 and 1050 cm^{-1}) are also visible in the spectra. The results obtained in this study are consistent with the literature and standard reference tables for the FTIR spectra of cellulose [25-27].

After chemical activation with phosphoric acid, the spectra of AC-50 and AC-85 show two main differences: (i)attenuation and broadening of cellulose markers (notably the glycosidic C–O stretches at 1160–1050 cm^{-1}), consistent with cleavage of glycosidic bonds and partial depolymerization/carbonization; and (ii) the emergence and intensification of absorptions in the 1250–900 cm^{-1} region assignable to P–O, P=O and P–O–C vibrations (phosphate esters, polyphosphate species or P-O–C linkages formed by phosphorylation of cellulose hydroxyls) [28].

AC-85 exhibits a larger suppression of cellulose marker bands (1160–1050 cm^{-1}), a more pronounced carbonyl shoulder (1700–1740 cm^{-1}), and stronger phosphate-region absorptions (1250–900 cm^{-1}) than AC-50. These differences indicate that increasing H_3PO_4 concentration promotes more extensive hydrolysis and dehydration during activation, a higher degree of phosphorylation/phosphate incorporation, and greater formation of oxygenated carbonyl species.

SEM Morphology

H_3PO_4 activation is known to both promote cleavage of the biopolymer chains and to introduce phosphorus-containing surface functionalities and crosslinking that template pore formation; higher acid concentration typically accelerates these reactions and produces more extensive porosity, provided that washing removes residual phosphates that could occlude pores [16,17,29]. To investigate how chemical activation and acid concentration affect the surface morphology of activated carbon samples, scanning electron microscopy (SEM) analysis was performed. Figure 3 shows the microscopic images of the prepared samples.

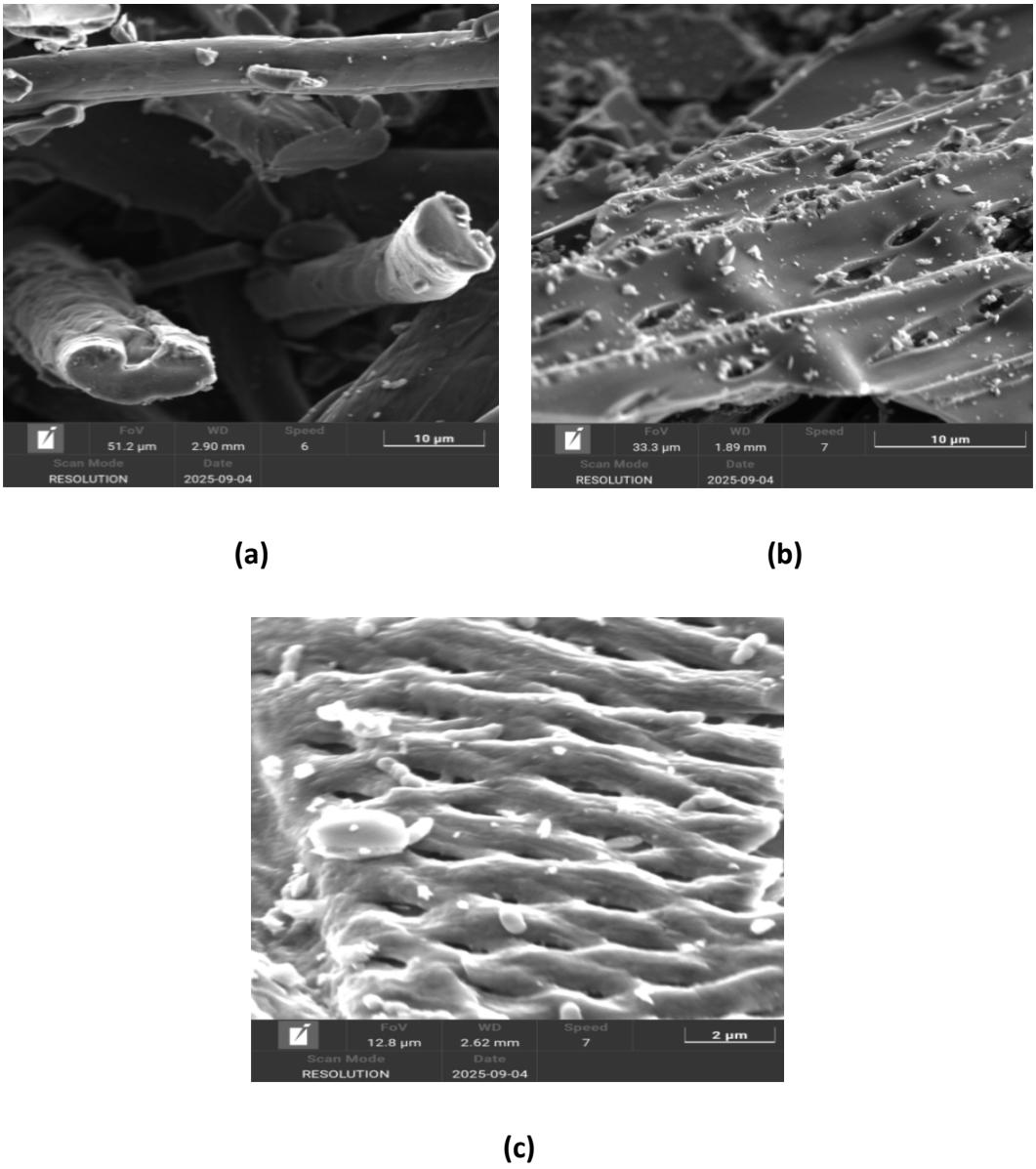

Figure 3. SEM images of (a) cotton waste, (b) AC-50, and (c) AC-85

SEM images show a gradual transformation of the raw cotton fibers into a porous carbon network with increasing concentration of H_3PO_4 used in chemical activation. The raw cotton waste (Figure 3a) retains its cellulose fiber structure, with smooth, cohesive surfaces exhibiting minimal fraying and some debris. No significant porosity is evident on the fiber surfaces, consistent with cotton fibers [30].

After chemical activation with 50 wt% H_3PO_4 (Fig. 3b), the fibers show clear signs of structural reorganization. The surface became roughened and partially collapsed, and a network of surface pits and irregular mesopores appeared. These features indicate partial decomposition of cellulose and the formation of accessible pores on the external surface. The pore geometry at this treatment level is heterogeneous: in

addition to small pits and crevices, isolated larger voids begin to appear, suggesting that acid impregnation and subsequent thermal treatment initiate both etching and cross-linking processes that open the surface. Similar mesopore formation upon H_3PO_4 activation has been reported for cotton-derived and other lignocellulosic precursors [30].

Increasing the activating agent concentration to 85 wt% (Fig. 3c) markedly intensifies these morphological changes. AC-85 exhibits a honeycomb-like surface with well-developed interlinked pores and thinned pore walls. The fiber skeleton is extensively broken down, producing broad pore channels and a more continuous porous network compared with AC-50. This progressive pore enlargement and interconnection with increasing H_3PO_4 concentration is consistent with enhanced dehydration, cleavage of glycosidic linkages and formation of phosphate-rich intermediates that catalyze char reorganization and pore development during carbonization [28,30].

The morphological evolution observed by SEM correlates qualitatively with expected changes in textural properties. The transition from intact fibers → roughened/partially porous surface (AC-50) → highly open, honeycomb-like network (AC-85) suggests increasing specific surface area and pore volume, and a shift toward a larger fraction of meso-/macropores that facilitate rapid ion transport — a desirable feature for electrode materials in supercapacitors.

Electrochemical Performance

The electrochemical studies were carried out in a two-electrode system with 1 M KNO_3 solution as electrolyte. The CV was conducted at different scan rates ranging from 1 mV s^{-1} to 1000 mV s^{-1} in a potential interval between 0 V and 0.8 V, which was intentionally selected as a conservative operating window to suppress electrolyte decomposition and ensure stable, reproducible capacitive behavior. The GCD tests were conducted over the same potential range at current densities ranging from 0.1 A.g^{-1} to 20 A.g^{-1}. The EIS measurements were conducted using an AC voltage in a frequency range of 0.01 Hz – 50 kHz at open-circuit potential. The specific capacitance C_{sp} (F g^{-1}) was calculated from the CV curves using Eq. 2:

$$C_{sp} = 2\frac{\int I\,dV}{m\,v\,\Delta V} \quad (2)$$

Where I (A) is the current, m (g) is the total mass of the two active electrodes, ν (V s^{-1}) is the scan rate, and ΔV (V) is the potential window

The GCD results were also used to calculate the specific capacitance C_{sp} (F g^{-1}) according to Eq. 3:

$$C_{sp} = 4\frac{I}{m\,(dV/dt)} \quad (3)$$

Where dV/dt (V s^{-1}) is the slope of the discharge curve.

Energy density (Wh kg^{-1}) and power density (W kg^{-1}) of the symmetric two-electrode supercapacitor were calculated according to Eq. 4 and Eq. 5, respectively:

$$E = C_{sp}\frac{\Delta V^{2}}{8 \times 3.6} \quad (4)$$

$$P = \frac{3600\,E}{t} \quad (5)$$

Where ΔV (V) is the effective potential range of the device during discharge and t (s) is the discharge time. Figure 4a and 4b show the CV curves of AC-50 and AC-85, respectively. Both samples exhibit a typical capacitive behavior with nearly rectangular-shaped CV at a low scan rate. This suggests that the prepared AC possesses an electric double-layer capacitive (EDLC) behavior and confirms the absence of significant faradaic redox peaks. With increasing scan rate, the CV curves become somewhat distorted and broadened, which is typically attributed to ion diffusion limitations and internal resistance within the porous structure [31,32]. The overall response remains capacitive even at high scan Figure 4c rates up to 1000 mV s^{-1}, indicating good reversibility and rapid ion transport within the pore network. Figure 4.c presents the specific capacitance of the two samples calculated using CV curves at different scan rates. The specific capacitance of AC-85 was found to be 135.6 $F.g^{-1}$ at 1 mV s^{-1}, while AC-50 exhibited a lower value of 108.1 $F.g^{-1}$ at the same scan rate.

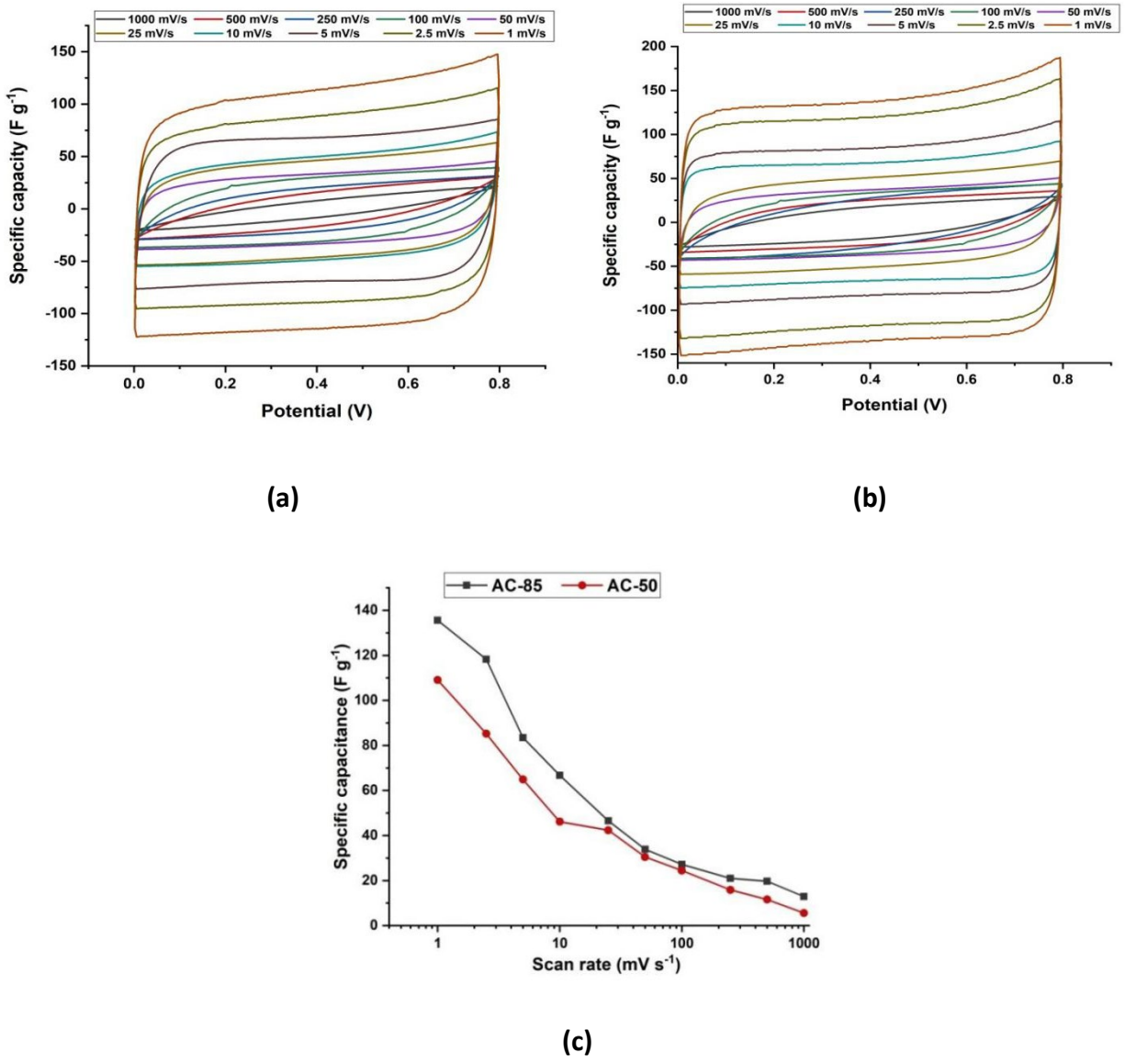

Figure 4. CV curves of AC electrodes: (a) AC-50, (b) AC-85, (c) variation of specific capacitance with scan rate

Furthermore, the GCD curves of the AC-50 and AC-85 were investigated and presented in Figure 5. AC-85 (Figure 5c,d) maintains nearly triangular potential–time profiles over the investigated current-density range and exhibits relatively small IR drops, indicating good electrochemical reversibility and efficient ion transport within the electrode. In contrast, AC-50 (Figure 5a,b) progressively deviates from ideal triangular behaviour as the current density increases, accompanied by shortened discharge times and higher IR drops, which can be attributed to enhanced ohmic resistance and kinetic limitations associated with ion diffusion in the porous structure. Quantitatively, AC-85 exhibits both higher low-rate capacitance and superior rate capability, retaining around 96% of its initial capacitance at 1 $A \cdot g^{-1}$, whereas AC-50 retains only 80% at the same current

density. These results indicate that stronger H_3PO_4 activation (85 wt%) produces a carbon material with a larger electrochemically accessible surface area, as commonly reported for phosphoric-acid-activated carbons, which facilitates rapid ion access at high current densities and mitigates diffusion resistance [30-32]. In accordance with the CV results, AC-85 therefore delivers higher specific capacitance and energy density than AC-50 across the examined current range. Consistent with the CV data, AC-85 also shows higher specific capacitance and energy density across the examined current range.

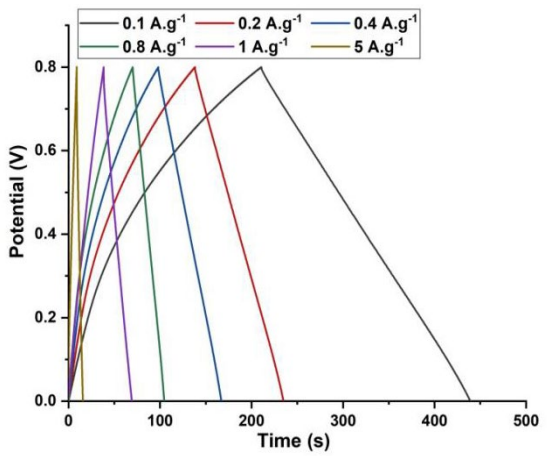

(a)

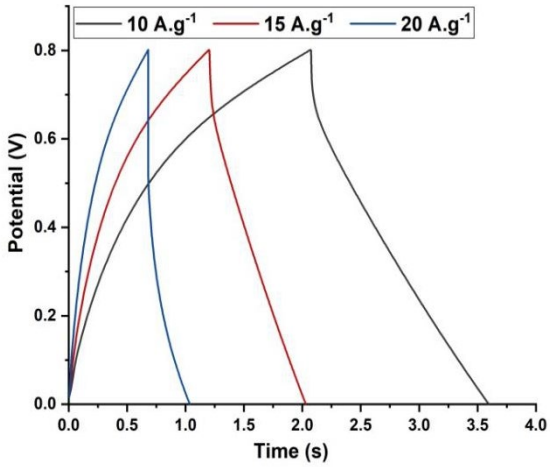

(b)

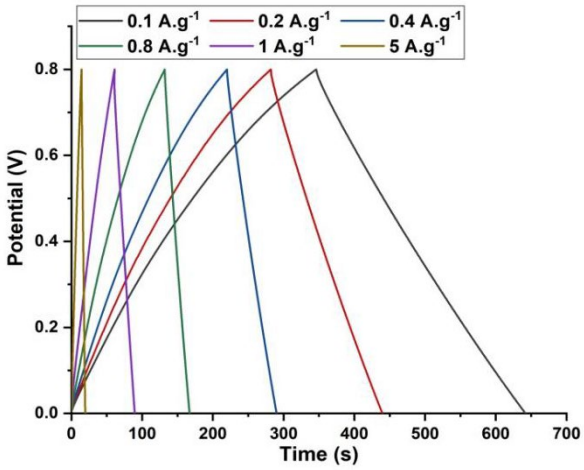

(c)

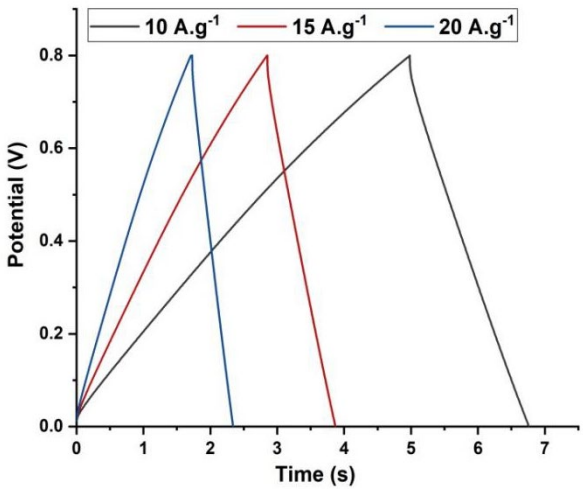

(d)

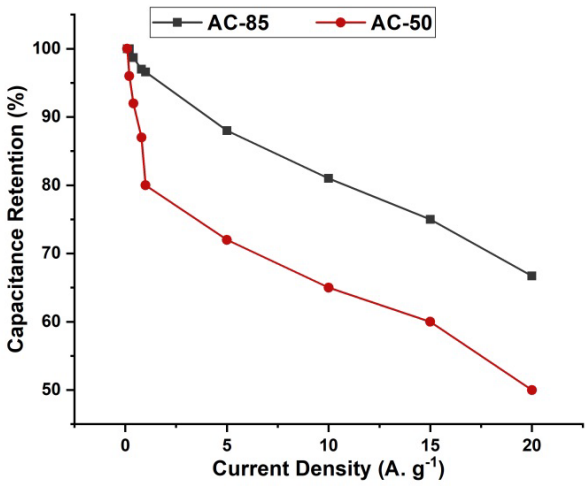

(e)

Figure 5. (a,b) GCD curves of AC-50 at different current densities, (c,d) GCD curves of AC-85 at different current densities, (e) capacity retention versus current density for both samples

The Ragone plot shown in Figure 6a clearly illustrates that the supercapacitor devices using the AC-85 electrodes exhibit much-enhanced energy/power density compared with the supercapacitors based on AC-50. Supercapacitor device prepared using AC-85 achieved an energy density of 3 Wh kg^{-1} at a power density of 40 W kg^{-1} and maintains 0.50 Wh kg^{-1} even at 3500 W kg^{-1}, while the device prepared using AC-50 provides 2.4 Wh kg^{-1} at a power density of 40 W kg^{-1} and 0.28 Wh kg^{-1} at 3000 W kg^{-1}. In this context, the enhanced energy density of AC-85 is attributed to a more developed porous structure resulting from stronger acid activation, which increases the number of available adsorption sites for electrolyte ions [31,32]. Although these energy values are lower than some literature reports, those often employ higher electrolyte concentrations, wider voltage windows, or modified electrode architectures that inherently boost performance and limit direct comparison [14,15]. Overall, both the CV and GCD performances suggest that AC-85 exhibits good specific capacitance in the aqueous electrolyte.

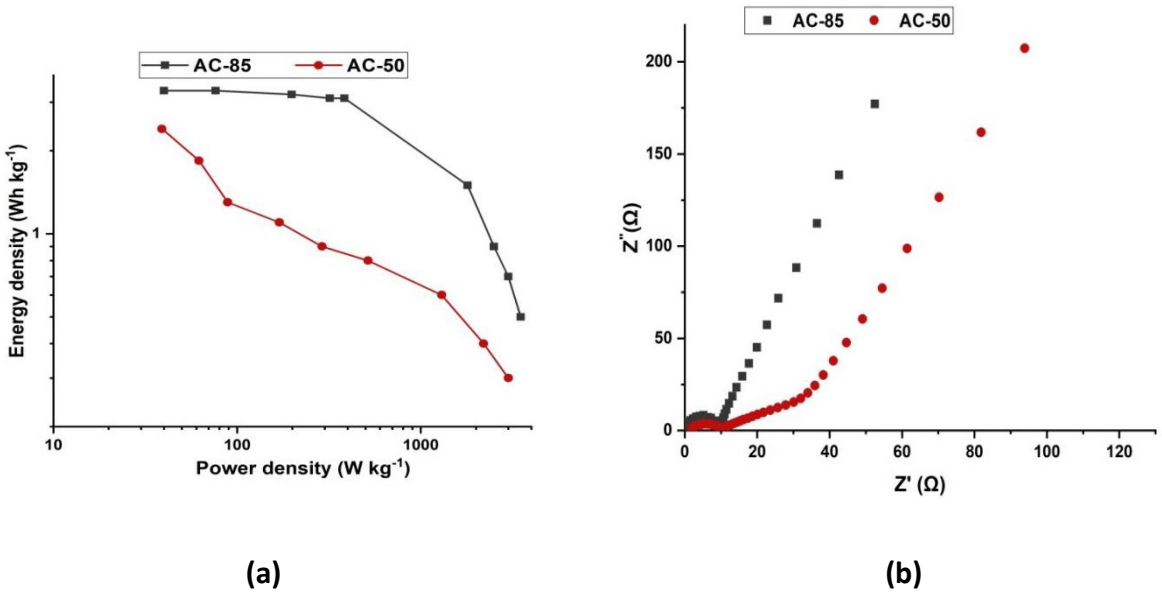

Figure 6. Electrochemical performance of the AC electrodes: (a) Ragone plot, (b) Nyquist plot

Additionally, electrochemical impedance spectroscopy (EIS) was used to test the series resistance and charge transfer resistance of the supercapacitor electrodes. The obtained Nyquist plots for the prepared AC samples are illustrated in Figure 6b, and the extracted impedance parameters are summarized in Table 2. Generally, supercapacitors exhibit resistive behavior at high frequencies and capacitive behavior at low frequencies. In a Nyquist plot, the high-frequency intercept on the real axis (Z') corresponds to the equivalent series resistance (ESR), which includes contributions from the electrode, electrolyte, and current collector. The semicircle observed in the high-to-medium frequency range is indicative of the charge transfer resistance (R_{ct}) at the electrode–electrolyte interface. At low frequencies, a vertical line represents ideal capacitive behavior, reflecting efficient ion diffusion and minimal resistive losses in the electrolyte [32].

The Nyquist plot of AC-50 shows a semicircle at high frequencies with a diameter corresponding to R_{ct}, followed by a gradually increasing line at low frequencies, indicating a slight deviation from ideal capacitive behavior due to limited ion accessibility within the porous structure. In contrast, AC-85 exhibits a nearly vertical line at low frequencies, with a much smaller semicircle at high frequencies, indicating both lower ESR and Rct values and faster charge transfer kinetics. This improved performance is consistent with the higher specific capacitance observed for AC-85, suggesting that increasing the H_3PO_4 concentration during activation enhanced the electrical conductivity [29-33].

Table 2. Impedance parameters extracted from the Nyquist plots of the AC electrodes

Sample	ESR (Ω)	R_{ct} (Ω)	Low-frequency slope (°)
AC-50	1.91	2.3	~70
AC-85	0.12	0.08	~85

Table 2 proves that AC-85 has significantly lower series and charge transfer resistance than AC-50, reflecting superior electrochemical kinetics and ion transport. At low frequencies, the slope of AC-85 approaches 90°, indicating more ideal capacitive behavior compared to AC-50. These results confirm that chemical activation with a higher H_3PO_4 concentration not only increases specific capacitance but also improves the electrode's conductivity and ion accessibility, making AC-85 a more promising candidate for high-performance supercapacitors.

CONCLUSION

This work shows that blow-room cotton waste can be successfully converted into AC for supercapacitor electrodes through phosphoric acid activation. The structural and electrochemical characteristics of the prepared AC were significantly improved when the H_3PO_4 concentration was increased from 50 wt% to 85 wt%. AC-85 exhibits lower volatile matter, higher fixed carbon content, and stronger phosphate-related surface functionalities compared with AC-50. Consequently, AC-85 shows a higher specific capacitance of 135.6 F g^{-1} at 1 mV s^{-1}, whereas AC-50 delivers 108.1 F g^{-1} at the same scan rate. Furthermore, AC-85 demonstrates better energy–power characteristics and markedly lower ESR and Rct. By demonstrating that blow-room waste can deliver competitive electrochemical performance, this study may open new opportunities for developing biomass-/waste-based AC for energy storage devices.

Author Contributions

Reem Shahin: Conceptualization, Methodology, Experimental Work, Data Processing, Formal Analysis, Writing - Original Draft.

Alexey Rodin: Supervision, Methodological Guidance, Validation of Results, Writing - Review and Editing, Project Management.

Conflicts of Interest

The authors declare no conflict of interest.

Funding

This research received no external funding.

Acknowledgements

This study was conducted in the Department of Physical Chemistry at the National University of Science and Technology MISiS. The researchers extend their sincere thanks to the department and the university for providing the materials and equipment necessary to complete this work.

REFERENCES

[1] Juanga-Labayen JP, Labayen IV, Yuan Q. A Review on Textile Recycling Practices and Challenges. Textiles. 2022; 2(1):174-188. doi: 10.3390/textiles2010010

[2] Habib A, Cozeli N, Babaarslan O, Kanat H, Tan S. Sustainable production of open-end rotor yarn for denim with maximum utilization of recycled cotton sourced from pre-consumer hard waste. Textile & Leather Review. 2024; 7:831–853. doi: 10.31881/TLR.2024.060

[3] Wannassi B, Kanan M, Hariz IB, Assaf R, Abusaq Z, Ben Hassen M, et al. Cotton Spinning Waste as a Microporous Activated Carbon: Application to Remove Sulfur Compounds in a Tunisian Refinery Company. Sustainability. 2023; 15(1):654. doi: 10.3390/su15010654

[4] Abtew MA, Atalie D, Dejene BK. Recycling of cotton textile waste: Technological process, applications, and sustainability within a circular economy. Journal of Industrial Textiles. 2025; 55:1–85. doi: 10.1177/15280837251348663

[5] Alcantara S, Moore F, Ontaneda M. A Systematic Review of Recycled Cotton Fibre Blending Practices, Challenges and Recommendations. Textile & Leather Review. 2024; 7:153–175. doi: 10.31881/TLR.2023.184

[6] Motin MM, Haq HM, Khan AN, Obaidur M, Rahman MO. Investigating the Ideal Combination of Virgin Cotton Fibre Length with Recycled Fibre for Better Yarn Quality. Textile & Leather Review. 2024; 7:391-402. doi: 10.31881/TLR.2024.009

[7] Subramaniam S, Karunanandham K, Raja ASM, Shukla SK, Uthandi S. EnZolv delignification of cotton spinning mill waste and optimization of process parameters using response surface methodology (RSM). Biotechnology for Biofuels and Bioproducts. 2024; 17:37. doi: 10.1186/s13068-024-02473-w

[8] Cho WS, Lee JH, Choi SS. Adsorbing odor via antibacterial activated carbon fiber derived from waste textiles. Macromolecular Research. 2025; 33(6):715-723. doi: 10.1007/s13233-024-00365-4

[9] Khan NA, Jahan Z, Iqbal N, Niazi MB, Mehek R. Synergistic electrochemical performance of textile sludge-based activated carbon with reduced graphene oxide as electrode for supercapacitor application. Waste Management. 2025; 191:274-283. doi: 10.1016/j.wasman.2024.11.015

[10] Venkatraman P, Aggarwal LM, Choudhary S, Jayachandran H, Chandrasekar S, Ambikapathi N, et al. Radiation Induced Activated Carbon from Coconut Shell for Supercapacitor Application. ChemistrySelect. 2025; 10(15):e202405919. doi: 10.1002/slct.202405919

[11] Singh S, Uppaluri R. Efficacy of double crucible method for the synthesis of activated carbon from rice husk. Biomass Conv. Bioref. 2025; 15:20463-20477. doi: 10.1007/s13399-025-06627-0

[12] Elattar MS, Kashyout AEB, Emara MM, Elbadawy HA, El-Sayed DS, Ali AE. High-yield green synthesis of carbon-nanohair/carbon quantum dots/activated carbon composite from agricultural or textile wastes for enhanced supercapacitor performance. Journal of Hazardous Materials. 2025; 207:112895. doi: 10.1016/j.jpcs.2025.112895

[13] Xia M, Shao X, Sun Z, Xu Z. Conversion of cotton textile wastes into porous carbons by chemical activation with $ZnCl_2$, H_3PO_4, and $FeCl_3$. Environmental Science and Pollution Research. 2020; 27(20):25186–25196. doi: 10.1007/s11356-020-08873-3

[14] Chen D, Li Z, Jiang J, Wu J, Shu N, Zhang X. Influence of electrolyte ions on rechargeable supercapacitor for high value-added conversion of low-grade waste heat. Journal of Power Sources. 2020;465:228263. doi: 10.1016/j.jpowsour.2020.228263

[15] Moyo B, Momodu D, Fasakin O, Bello A, Dangbegnon J, Manyala N. Electrochemical analysis of nanoporous carbons derived from activation of polypyrrole for stable supercapacitors. Journal of Materials Science. 2018; 53:5229–5241. doi: 10.1007/s10853-017-1911-y

[16] Liu W, Wu F, Fan M, Zhang S, Wang S, Hu X. Activation of poplar with H_3PO_4 and H_2SO_4: Synergistic effects of dual acids on pore development of activated carbon for enhanced adsorption of phenol and tetracycline. Colloids and Surfaces A: Physicochemical and Engineering Aspects. 2025; 393:138861. doi: 10.1016/j.colsurfa.2025.138861

[17] Dhandapani E, Kandiah K, Arumugam G, Rajendran R, Duraisamy N. Hierarchically porous activated carbon electrodes synthesized from expired tablets for high-performance supercapacitor and photocatalysis application. Journal of Materials Science: Materials in Electronics. 2025; 36:589. doi: 10.1007/s10854-025-14654-w

[18] Neme I, Gonfa G, Masi C. Activated carbon from biomass precursors using phosphoric acid: A review. Heliyon. 2022;8(12):e11940. doi: 10.1016/j.heliyon.2022.e11940

[19] Lee SY, Kim JG, Jun YS, Park YI. Sustainable utilization of cellulose-rich corn husk for activated carbon in high-performance sodium-ion capacitors. Applied Surface Science. 2025; 695:162916. doi: 10.1016/j.apsusc.2025.162916

[20] Bamerdhah SS, Kumar NS, Al-Ghurabi EH, Boumaza M, Asif M. Optimized synthesis of activated carbon from date palm seeds for efficient crude oil adsorption in wastewater treatment. Scientific Reports. 2025; 15(1):31122. doi: 10.1038/s41598-025-16831-7

[21] ASTM International. Standard D2867-23 - Standard Test Methods for Moisture in Activated Carbon. 2023. doi: 10.1520/D2867-23

[22] ASTM International. Standard D5832-98R14 – Standard Test Method for Volatile Matter Content of Activated Carbon Samples. 2014. doi: 10.1520/D5832-98R14

[23] ASTM International. Standard D2866-11R18 - Standard Test Method for Total Ash Content of Activated Carbon. 2018. doi: 10.1520/D2866-11R18

[24] Tay T, Ucar S, Karagöz S. Preparation and characterization of activated carbon from waste biomass. Journal of Hazardous Materials. 2009; 165(1-3):481-485. doi: 10.1016/j.jhazmat.2008.10.011

[25] Ibrahim M, Souleiman M, Salloum A. Methylene blue dye adsorption onto activated carbon developed from Calicotome villosa via H_3PO_4 activation. Biomass Conversion and Biorefinery. 2023; 13(14):12763-12776. doi: 10.1007/s13399-021-02027-2

[26] Serafin J, Roman-Martínez MC, Srenscek-Nazzal J, Dziejarski B, Yahia E, Cherif EK, et al. Preparation of activated carbon from Moroccan argan press cake using KOH activation and its application for CO_2 adsorption. Fuel. 2025; 393:134922. doi: 10.1016/j.fuel.2025.134922

[27] Al Lafi AG, Khuder A. Removal of Cr (VI) from aqueous solutions by activated carbon and its composite with $P_2W_{17}O_{61}$: A spectroscopic study to reveal adsorption mechanism. Heliyon. 2025; 11(2):e41862. doi: 10.1016/j.heliyon.2025.e41862

[28] Al-Kaabi MA, Zouari N, Al-Ghouti MA. Novel insights into date pit-based activated carbons: H_3PO_4 and KOH activation. Arabian Journal of Chemistry. 2025; 18:202025. doi: 10.25259/AJC_20_2025

[29] Ukanwa KS, Patchigolla K, Sakrabani R, Anthony E, Mandavgane S. A Review of Chemicals to Produce Activated Carbon from Agricultural Waste Biomass. Sustainability. 2019; 11(22):6204. doi: 10.3390/su11226204

[30] Heidarinejad Z, Dehghani MH, Heidari M, Javedan G, Ali I, Sillanpää M. Methods for preparation and activation of activated carbon: A review. Environmental Chemistry Letters. 2020; 18(2):393–415. doi: 10.1007/s10311-019-00955-0

[31] Chen G, Lu B, Li J, Wu C, Xiao Y, Dong H, et al. Regulating medical wasted cotton into porous carbons for high-performance supercapacitors and zinc-ion hybrid capacitors. Journal of Power Sources. 2024; 599:234146. doi: 10.1016/j.jpowsour.2024.234146

[32] Dai P, Zhang S, Liu H, Yan L, Gu X, Li L, et al. Cotton fabrics-derived flexible nitrogen-doped activated carbon cloth for high-performance supercapacitors in organic electrolyte. Electrochimica Acta. 2020; 354:136717. doi: 10.1016/j.electacta.2020.136717

[33] Manimekala T, Sivasubramanian R, Dar MA, Dharmalingam G. Crafting the architecture of biomass-derived activated carbon via electrochemical insights for supercapacitors: A review. RSC Advances. 2025; 15(4):2490-2522. doi: 10.1039/D4RA07682F